Journal of Materials Chemistry A

Accepted Manuscript

This is an *Accepted Manuscript*, which has been through the Royal Society of Chemistry peer review process and has been accepted for publication.

Accepted Manuscripts are published online shortly after acceptance, before technical editing, formatting and proof reading. Using this free service, authors can make their results available to the community, in citable form, before we publish the edited article. We will replace this *Accepted Manuscript* with the edited and formatted *Advance Article* as soon as it is available.

You can find more information about *Accepted Manuscripts* in the Information for Authors.

Please note that technical editing may introduce minor changes to the text and/or graphics, which may alter content. The journal's standard Terms & Conditions and the Ethical guidelines still apply. In no event shall the Royal Society of Chemistry be held responsible for any errors or omissions in this *Accepted Manuscript* or any consequences arising from the use of any information it contains.

ROYAL SOCIETY OF CHEMISTRY

www.rsc.org/materialsA

Journal of Materials Chemistry A Accepted Manuscript

Table of Contents Graphic

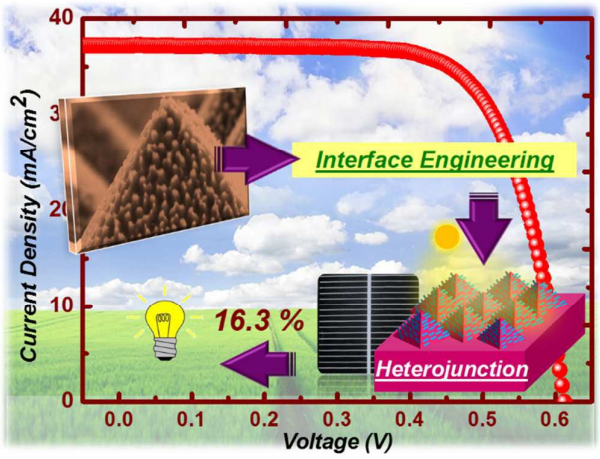

With a system of interface engineering treatment, heterojunction solar cells fabricated with hierarchical nanostructures exhibit the efficiency of 16.3% using cost-effective as-cut Czochralski n-type silicon substrates.

Increasing Efficiency of Hierarchical Nanostructured Heterojunction Solar Cells to 16.3% via Controlling Interface Recombination

Fengyou Wang[†‡], Yuanjian Jiang[†], Tiantian Li[†], Ying Zhao[†‡] and Xiaodan Zhang[†‡*]

[†]Institute of Photo-electronics Thin Film Devices and Technique of Nankai University, Key Laboratory of Photo-electronics Thin Film Devices and Technique of Tianjin, 300071, P. R. China

[‡]Collaborative Innovation Center of Chemical Science and Engineering (Tianjin), Tianjin, 300072, P. R. China

Corresponding Author

*Xiaodan Zhang, Email address: xdzhang@nankai.edu.cn

Journal of Materials Chemistry A Accepted Manuscript

ABSTRACT

Silicon nanostructures show great promise for use in photovoltaic applications, owing to their enhanced light-harvesting characteristics, which allow them to form radial p-n junctions for effectively generating/separating photoexcited carriers. They are also low-cost materials and thus suitable for producing solar cells. In this study, hierarchical Si structures consisting of microscaled pyramids and nanoscaled pillars were fabricated through wet anisotropy texturing and reactive ion etching. Further, these substrates, which had a core-shell structure, were used to fabricate radial heterojunction Si solar cells through interface engineering with tetramethylammonium hydroxide. The substrates were pretreated with a hydrogen plasma and subsequently subjected to amorphous Si thin-film passivation. This resulted in solar cells with a markedly higher broadband wavelength; however, the electrical properties of the cells almost remained unaffected. Further, the heterojunction solar cells, which had a hierarchical nanostructure and were fabricated using as-cut Czochralski n-type Si substrates, exhibited an efficiency of 16.3%, which is the highest ever reported for such cells.

KEYWORDS: nanopillars, solar cells, radial junction, surface passivation, heterojunction

Journal of Materials Chemistry A Accepted Manuscript

Introduction

The ability to effectively trap light in photovoltaic devices has become critical, given the continuous improvements in cell design by coupling as much light as possible into the cells for improving cell efficiency [1-6]. These improvements are attributable to the use of nanostructured materials in the cells, which improve the optical as well as the electrical properties of the cells through their unique architectures [7-9]. With respect to the optical properties, vertically aligned nanoarrays are known to suppress light reflection. This effect can be attributed to the nanotexture of the arrays, which results in an increase in the optical path length for guided-mode coupling [10]. Further, in the case of the electrical properties, the vertical junction of radial diodes provides a collection path separated from the photoexcited thickness; thus, while the charge carriers are collected along the radial direction, photons are absorbed along the height of the nanostructures [11]. The orthogonal separation of sunlight and the diffusion of minority carriers are conducive to the diffusion of carriers over short distances in the case of p-n junctions, allowing the carriers to be extracted with minimal recombination within the bulk of the Si material. However, before these advantages can be exploited in practice, a few key aspects need to be considered, and some design challenges need to be addressed. In particular, the ultrahigh surface area of these nanostructures results in an increase in the density of the surface defects, causing the recombination velocity (S_{it}) to be high. Although photoexcited carriers can be transported rapidly to the junction interface, they are readily trapped by surface defects, which are present in a high density, before being collected by the external circuit. The electrical advantages of the radial junction architecture are thus mitigated by the high S_{it}, resulting in performance deterioration and causing the open-circuit voltage (V_{oc}), fill factor (FF), and short-circuit density (J_{sc}) values to be low. Thus, the interface should be engineered appropriately, in

Journal of Materials Chemistry A Accepted Manuscript

order to overcome these issues. Jia et al. [12] could suppress surface recombination by depositing an ultrathin passivating Al_2O_3 tunnel layer on a highly doped p-type a-Si:H emitter layer, which resulted in an efficiency of 10.04%. Kim et al. [13] have fabricated hybrid Si radial nanowires-based solar cell with an efficiency of 11% by passivating the top surface and the p-n junction with thin a-SiN: H and intrinsic poly-Si films, respectively. In contrast, in this study, we report a p-n heterojunction solar cell based on hierarchical architecture Si wafers, which consisting of randomly distributed micropyramids (MPs) and nanopillars (NPs). Light management using these hierarchical structures resulted in significantly improved photoharvesting characteristics. We used wide-bandgap, intrinsic hydrogenated amorphous Si (i-a-Si:H) for the passivation layer and boron-doped a-Si:H (p-a-Si:H) for the emitter layer, in order to demonstrate the concept of the heterojunction, while focusing on the interface-engineering aspect of the devices. Further, in order to reduce the density of surface defects in the substrates, a hydrogen plasma pretreatment and a chemical etching treatment with an organic aqueous solution of tetramethylammonium hydroxide (TMAH) were employed. This prevented inhomogeneous a-Si:H deposition, residual metal contamination, and the formation of excessive carrier-trapping centers owing to a high density of surface defects. By employing these techniques concurrently for the interface passivation of the solar cell with Si MPs+NPs structure heterojunction, the external quantum efficiency (*EQE*) at short wavelengths could be increased significantly. A V_{oc} of 611 mV, *FF* of 71.7%, J_{sc} of 37.1 mA/cm^2, and a conversion efficiency of 16.3% were observed for the cell with the Si nanostructured heterojunction (details related to the performance of the cell are listed in Table S1).

Experimental section

Substrate cleaning. As a pre-deposition surface cleaning step, all the samples were treated with

Journal of Materials Chemistry A Accepted Manuscript

acetone/methanol/deionized water and then subjected to the RCA cleaning procedure. Before being transported to the deposition chamber, the wafers were dipped in 1% hydrofluoric acid for 3 min, in order to pre-saturate the surface dangling bonds and remove the native oxide layer. After being blow dried with nitrogen, the samples were transported immediately to the load lock of the deposition system, in order to prevent oxidation and contamination by other materials.

Solar cell fabrication. The p-a-Si: H and n-a-Si: H films were deposited in separate chambers of a plasma-enhanced chemical vapor deposition (PECVD) system at 180°C. The p-a-Si:H films were prepared in the front using a gaseous mixture of silane (SiH_4), trimethylboron, and H_2. The n-a-Si: H films were prepared in the rear using a gaseous mixture of SiH_4, phosphine (PH_3), and H_2. The thickness of the Ag grid (in the front) and the back contact were both set to ~600 nm. Indium tin oxide (ITO) layers (~80 nm in thickness) were patterned by physical vapor deposition onto a 1 cm^2 pad area. The current density–voltage (*J*–*V*) characteristics of the solar cells were measured at 25°C under 1 sun illumination (AM1.5; 100 mW/cm^2) from a solar simulator.

Device characterization. The *J*–*V* characteristics of the photovoltaic devices under illumination were measured with an AAA grade Wacom solar simulator (WXS-156S-L2, AM1.5GMM). The spectral responses were obtained using a quantum efficiency measurement system (QEX10, PV Measurement), which was equipped with a monochromator, lock-in amplifier, Xe lamp, and current–voltage amplifier. The surface morphologies of the textured wafers were analyzed using scanning electron microscopy (SEM) (ZEISS SUPRA 55VP). The surface reflectances of the textured wafers were determined using a Varian-Cary 5000 ultraviolet-visible-near-infrared integrating sphere spectrophotometer. X-ray photoelectron

Journal of Materials Chemistry A Accepted Manuscript

spectroscopy (XPS) was performed using a PHI5000 Versa Probe, and the effective carrier recombination rate was evaluated from the minority carrier lifetime using the quasi-steady-state photoconductance (QSSPC) technique; the Sinton WCT-120 silicon lifetime and wafer metrology system was employed for the purpose.

Results and discussion.

Usually, for large-scale photovoltaic application, commercial, as-cut, and monocrystalline n-type Si (100) Czochralski wafers (150 μm) are used, as they are more cost effective compared to the floating-zoning Si wafers with higher carrier lifetimes [14,15]. Fig. 1a-c show SEM images representing the morphology evolution of the Si hierarchical architecture during the etching process. The Si MPs were formed on the 51-mm-diameter wafers via anisotropic etching with a solution of 1% sodium hydroxide (NaOH) and 6% isopropyl alcohol. After etching for 30 min, randomly distributed MPs with a size of 6–8 μm were formed on the Si surface, as shown in Fig. 1a. Subsequently, as shown in Fig. 1b, a 15-nm-thick Ag thin film was deposited on the surfaces of the MPs via magnetron sputtering. This was followed by annealing for 40 min at 260 °C in air. This resulted in the self-aggregation of Ag nanodots on the surfaces of the MPs. Next, by using the randomly distributed Ag nanodots, which had a size of ~150–350 nm, as a nanomask, the Si substrates were dry etched with a planar-type reactive ion etching (RIE) system at a frequency of 13.56 MHz and bias power of 70 W. The chamber pressure was kept at 10 Pa during the 2-min etching process, and the etching gas, SF_6, was introduced into the reactive chamber to form the hierarchical architectures. After the completion of the RIE process, the wafers were dipped in HNO_3 for 30 s to remove the mask of Ag nanodots and then cleaned in deionized water. Figure S1 shows photographic images of the three kinds of Si substrates; the

Journal of Materials Chemistry A Accepted Manuscript

fact that samples exhibit a uniform color distribution suggests that this method is suitable for industrial production. Finally, the samples were treated with acetone/methanol/deionized water and then subjected to the RCA cleaning procedure. The top and sectional views of the substrates after the RIE process are shown in Figs. 1c and d, respectively.

Next, we examined the effects of light absorption at wavelengths of 300–1200 nm on the substrates with the planar, Si MPs, and Si MPs+NPs hierarchical architectures, as shown in Fig. 1e. The absorption percentages were calculated by measuring the hemispheric integrated transmittances and reflectances of the wafers. Compared to the planar substrate, those with the Si MPs and Si MPs+NPs hierarchical architectures absorbed markedly higher amounts of light at wavelengths of 300–1000 nm; this was mainly attributable to the high degree of light trapping (i.e., low reflectance) at the front sides of the wafers by the MPs and MPs+NPs, as shown in Fig. S2. Interestingly, for wavelengths higher than 1000 nm, there continued to be differences in the amounts of light absorbed by the planar substrate and the other two substrates. Nevertheless, the absorptions of the Si MPs and Si MPs+NPs wafers at wavelengths higher than 1000 nm were almost identical, and the normalized increase in absorption was reduced to ~0%, as shown in Fig. S3. For wavelengths greater than 1000 nm, the size of the nanostructures was smaller than the smallest wavelength. Thus, the front-side nanostructures could not trap light effectively, as the heights of the NPs were 500–700 nm. Therefore, the fact that the absorptions of the Si MPs and Si MPs+NPs substrates were similar for longer wavelengths can be attributed to the fact that the two wafers had similar MPs on the rear side, in contrast to the case for the planar wafer, as shown in the inset of Fig. 1e. The MPs resulted in a higher degree of scattering at the front and rear sides at long wavelengths (> 1000 nm) [16,17]; this increased the total path length for effective light absorption within the wafers.

Journal of Materials Chemistry A Accepted Manuscript

To evaluate the feasibility of managing light absorption using the light-harvesting hierarchical structures and converting the trapped photons into electrons, a typical p-i-n core/shell Si MPs+NPs solar cell (shown in Fig. 2a) was fabricated by PECVD (details of the PECVD process are given in Supporting Information in Tables S2 and S3); a high-vacuum (10^{-6} to 10^{-8} Pa) multichamber cluster PECVD system was employed for the purpose. The structure of the solar cell was as follows: Ag grid/ITO/p-type a-Si:H/i-a-Si:H/n-type Si MPs+NPs/i-a-Si:H/n-type a-Si:H/ITO/Ag electrode. The i-a-Si:H layer at the bifacial of the substrate resulted in good chemical passivation, minimizing the surface recombination loss. Before the deposition of the a-Si:H layer, a 60 s hydrogen plasma pretreatment was performed, in order to saturate the dangling bonds on the wafer surface. This also improved the homogeneity of the subsequently deposited a-Si:H layers, thus improving the degree of passivation of the a-Si:H/c-Si interface. The working mechanism of this process has been reported previously [18]. Figure 2b shows the EQE curves of the three solar cells for wavelengths of 300–1200 nm, while their *J-V* characteristics are summarized in Table 1. The J_{sc} values of the solar cells were calculated with EQE by integrating with AM1.5G solar spectrum and not by measuring the *J-V* characteristics directly, in order to avoid the lateral collection effect. It can be observed that the J_{sc} values of the substrates with the planar and Si MPs structures were 30.7 and 35.9 mA/cm^2, respectively, while that of the substrate with the Si MPs+NPs hierarchical structure was 36.6 mA/cm^2. Thus, there was a significant increase for short wavelengths from the planar solar cell to the one with the MPs+NPs hierarchical structure (see the green region of Fig. 2b). On the other hand, for longer wavelengths (> 1000 nm), the performances of the Si MPs and Si MPs+NPs solar cells were similar and better than that of the planar one. This was in accordance with the amounts of light absorbed by these substrates, as shown in Fig. 1e. However, even

Journal of Materials Chemistry A Accepted Manuscript

though the substrate with the Si MPs+NPs structure exhibited a higher light-trapping ability, as shown in Table 1, both the V_{oc} value and the *FF* value of this cell were lower which cause the conversion efficiency of the solar cell based on MPs+NPs structure was lower than that of the cell based on the MPs structure. This phenomenon implies that the carrier recombination rate of the cell based on the MPs+NPs structure was high, offsetting the advantages of its high light-trapping ability. That is to say, the contribution of the MPs+NPs light-harvesting structure was mitigated by the electrical deterioration caused by this structure, owing to the increase in the shunting current within the space-charge region.

In fact, during the fabrication of the Si MPs+NPs structure, the substrate surface was subjected to bombardment by high-powered ions during the RIE process; this would have induced the breakage of the surface Si-Si bonds, thus increasing the number of surface dangling bonds and the density of defects. In addition, although the Ag nanodots were removed by HNO_3 and a subsequent RCA cleaning process, residual Ag^+ ions on the surface probably continued to exist at the bottom of the NPs, owing to the hydrophobicity of etched Si surfaces [19]. Depositing a-Si:H on the as-processed Si MPs+NPs substrate resulted in a shunted device. Further, contamination by the Ag^+ ions probably led to deep-energy-level defects on the surface, increasing the S_{it} value of the device. To ensure high V_{oc} values, one needs to fabricate the interface carefully, so that it allows for effective carrier collection; this is not the case with defective interfaces and those corresponding to high S_{it} values. The relation between V_{oc} and S_{it} can be expressed as [20]

$$V_{oc} = \frac{\phi_B}{q} - \frac{nkT}{q}\ln\left(\frac{qN_v S_{it}}{J_{sc}}\right) \qquad (1)$$

Journal of Materials Chemistry A Accepted Manuscript

where ϕ_B is the effective barrier, q is the elementary charge, kT is the thermal energy, and N_V is the effective density of states in the valence band. It can be concluded from Eq. (1) that a decrease in S_{it} (i.e., an increase in the effective minority carrier lifetime) would increase the V_{oc} value of the device. Therefore, it is necessary to create an atomically smooth surface and remove the contaminating Ag^+ ions, such that the formed hierarchical structure results in a decrease in S_{it}. In this study, we modified the Si MPs+NPs substrate with a low-concentration aqueous TMAH solution to achieve this effect. TMAH is an organic alkali etchant. Further, it is nonpoisonous, does not cause contamination by metal ions, results in a high degree of anisotropic etching, and is well suited for use with microelectronic devices.

Figure 3a shows the minority carrier lifetimes for the different substrates passivated by 10-nm-thick i-a-Si:H films and characterized by the QSSPC technique. The planar structure exhibited a lower carrier lifetime than did the Si MPs structure; this was owing to the large number of (100) planes exposed in the case of the planar structure. The (100) plane exhibits two kinds of dangling bonds, while the (111) plane exhibits only one type [21], leading to the surface state density of the (100) plane being higher than that of the (111) plane. Therefore, during i-a-Si:H deposition, the high dangling bond density on the (100) plane wafer reducing the a-Si:H precursor diffusion coefficient, resulting high-defects Si thin films occurs more readily on high-defect-density (100) planes than on (111) planes [22, 23]. This resulted in the formation of a large number of defects, leading to a large number of recombination centers at the grain boundaries of the network matrices of the films. This significantly retarded the surface passivation effects and decreased the minority carrier lifetime, thus lowering the V_{oc} value of the solar cell. In contrast, after the anisotropic texturing of the wafer with the MPs, mainly (111) crystals were exposed on the pyramid facets; these were more suitable for forming abrupt a-

Journal of Materials Chemistry A Accepted Manuscript

Si:H/c-Si interfaces without epitaxial growth [24] and thus for lowering the surface recombination rate. As a result, the carrier lifetime for the MPs structure was the highest. On the other hand, the Si MPs+NPs structure not treated with TMAH exhibited the smallest minority carrier lifetime, owing to the fact that the surface area of the MPs+NPs structure was high and because fewer (111) planes were exposed. This increased the recombination rate for the minority carriers. Further, a large number of defects were formed on the wafer surface, which was also contaminated with Ag^+ ions.

In particular, one can see that the lifetime increased significantly, from 192 μs to 447 μs (corresponding to an excess carrier density of 10^{15} cm^{-3}) after the TMAH treatment of the MPs+NPs substrate. This increase in the lifetime may be attributed to the effective reduction of the surface defects and the atomic smoothening of the Si surface, which decreased the density of recombination centers at the a-Si:H/c-Si interface and significantly improved the quality of the interface [25,26]. In addition, as shown in Fig. 3b, the results of XPS indicated that the TMAH treatment removed the residual Ag^+ ions from the Si surface. The concentration of the residual Ag^+ ions decreased from 0.18 at% before the TMAH treatment to 0 at% after the treatment.

To evaluate the effects of the TMAH treatment on the solar cell properties, we fabricated solar cells using the TMAH-treated substrates. The fabrication process was identical to the one used previously. Figure S4 in the supporting information have presented the total reflectance of the solar cells based on different substrates. One can see that the optical properties of the solar cell based on the substrates with and without TMAH treatment was almost identical. The *J-V* curves of the solar cells based on the untreated and TMAH-treated substrates under AM 1.5 illumination are shown in Fig. 4a. It can be seen that the solar cell based on the treated substrate exhibited markedly improved performance in terms of the V_{oc}, J_{sc}, and *FF* values. The cell based

Journal of Materials Chemistry A Accepted Manuscript

on the treated substrate exhibited a power conversion efficiency of 15.9±0.4 %, the highest efficiency could be 16.3 % (V_{oc} = 611 mV, J_{sc} = 37.1 mA/cm^2, and *FF* = 71.7%); In contrast, the one fabricated on the untreated substrate had an efficiency of 14.2±0.5%, the highest efficiency could be 14.7 % (V_{oc} = 573 mV, J_{sc} = 36.6 mA/cm^2, and *FF* = 70.1%). A substantial increase in EQE was also observed after the TMAH treatment, as shown in Fig. 4b. Given that identical substrates were used for the solar cells and that the PECVD deposition conditions were the same, the low carrier-collection efficiency in case of the cell fabricated on the untreated substrate is attributable to the high density of surface defects and the metal contamination of the untreated surface. Further, because TMAH has a low ionic polarity [27], the surfaces of the Si MPs and NPs became smoother after the TMAH treatment [28-30], allowing for the deposition of a more uniform a-Si: H passivation layer. More importantly, as reported by other groups, we speculated that the atomically rough surfaces can act as nucleation sites for defects-rich Si growth during a-Si: H film deposition, resulting in a low degree of surface passivation [31-33]. The smoothening of the surfaces after the TMAH treatment lowered the chances of this happening, thus decreasing the dark current density significantly. Figure 4c shows the dark *J-V* characteristics of the solar cells formed on the untreated and treated substrates to explore the quality of the p-n junction. The dark current under forward bias voltage for the solar cell based on the treated substrate was lower than that of the cell based on the untreated substrate. On the basis of semiconductor device physics, increases in the dark current at low forward biases (< 0.5 V) can be attributed directly to an increase in the recombination rate in the depletion region as well as an increase in the shunting path within the p-n junction. Moreover, the electrical current of the p-n junction under reverse bias voltage also indicated that the device fabrication with TMAH treatment has less leakage current within the p-n junction.

Journal of Materials Chemistry A Accepted Manuscript

Conclusions

In summary, we developed an effective approach for fabricating hierarchically structured, heterojunction Si solar cells by using wet anisotropic etching and dry RIE to form MPs and NPs, respectively. The hierarchically structured Si MPs+NPs substrate exhibited better light absorption at wavelengths of 300–1100 nm than the planar and Si MPs substrates. An interface-control technique was employed to prevent the electrical properties of the solar cells from being affected adversely. A treatment with low-concentration TMAH was used to modify the surfaces of the hierarchically structured Si substrates, in order to minimize the number of defects and to remove contaminating metal ions. This resulted in an improvement in the minority carrier lifetime. When used in combination with a hydrogen plasma pretreatment and a-Si:H thin-film passivation, this technique resulted in n-type nanostructure heterojunction Si solar cells that could exhibit an efficiency as high as 16.3%. Both the substrate fabrication method and the interface modification technique employed in this study should be suitable for use with a wide range of coating materials and substrates and should aid in the development of practical high-efficiency nanostructured solar cells.

Acknowledgment

The authors gratefully acknowledge the supports from Key Project in the Science & Technology Pillar Program of Jiangsu Province (BE2014147-3) and Ph.D. Candidate Research Innovation Fund of Nankai University (68150003).

References

[1] A. Mavrokefalos, S. E. Han, S. Yerci, M. S. Branham, G. Chen, Nano Lett. 12 (2012) 2792-2796.

[2] Y. Liu, A. Das, Z. Lin, I. B. Cooper, A. Rohatgi, C. P. Wong, Nano Energy 3 (2014) 127-133.

Journal of Materials Chemistry A Accepted Manuscript

[3] S. Sridharan, N. Bhat, K. N. Bhat, Appl. Phys. Lett. 102 (2013) 021604.

[4] X. X. Lin, X. Hua, Z. G. Huang, W. Z. Shen, Nanotechnology 24 (2013) 235402.

[5] F. Voigt, T. Stelzner, S. Christiansen, Prog. Photovoltaics 21 (2013) 1567-1579.

[6] I. Kim, D. S. Jeong, W. S. Lee, W. M. Kim, T.-S. Lee, D.-K. Lee, J.-H. Song, J.-K. Kim, K.-S. Lee, Opt. Express 22 (2014) A1431.

[7] Z. Fan, D. J. Ruebusch, A. A. Rathore, R. Kapadia, O. Ergen, P. W. Leu, A. Javey, Nano Res. 2 (2009) 829-843.

[8] S. E. Han, G. Chen, Nano Lett. 10 (2010) 1012-1015.

[9] J. Y. Kwon, D. H. Lee, M. Chitambar, S. Maldonado, A. Tuteja, A. Boukai, Nano Lett. 12 (2012) 5143-5147.

[10] G.-J. Lin, H.-P. Wang, D.-H. Lien, P.-H. Fu, H.-C. Chang, C.-H. Ho, C.-A. Lin, K.-Y. Lai, J.-H. He, Nano Energy 6 (2014) 36-43.

[11] Y. Cui, M. L. Charles, Science 291 (2001) 851-853.

[12] G. Jia, B. Eisenhawer, J. Dellith, F. Falk, A. Thøgersen, A. Ulyashin, J. Phys. Chem. C 117 (2013) 1091-1096.

[13] D. R. Kim, C. H. Lee, P. M. Rao, I. S. Cho, X. Zheng, Nano Lett. 11 (2011) 2704-2708.

[14] B. Stegemann, J. Kegel, M. Mews, E. Conrad, L. Korte, U. Stürzebecher, H. Angermann, Energy Procedia 38 (2013) 881-889.

[15] D.-H. Neuhaus, A. Münzer, Adv. OptoElectron. 2007 (2007) 1-15.

[16] K. X. Wang, Z. Yu, V. Liu, Y. Cui, S. Fan, Nano Lett. 12 (2012) 1616-1619.

[17] A. Ingenito, O. Isabella, M. Zeman, ACS Photonics 1 (2014) 270-278.

[18] F. Wang, X. Zhang, L. Wang, Y. Jiang, C. Wei, J. Sun, Y. Zhao, ACS Appl. Mater. Interfaces 6 (2014) 15098-15104.

Journal of Materials Chemistry A Accepted Manuscript

[19] H.-P. Wang, T.-Y. Lin, C.-W. Hsu, M.-L. Tsai, C.-H. Huang, W.-R. Wei, M.-Y. Huang, Y.-J. Chien, P.-C. Yang, C.-W. Liu, L.-J. Chou, J.-H. He, ACS Nano 7 (2013) 9325-9335.

[20] M. Mikolášek, J. Racko, L. Harmatha, P. Gašpierik, P. Šutta, Appl. Surf. Sci. 256 (2010) 5662-5666.

[21] U. K. Das, M. Z. Burrows, M. Lu, S. Bowden, R. W. Birkmire, Appl. Phys. Lett. 92 (2008) 063504.

[22] M. Algasinger, J. Paye, F. Werner, J. Schmidt, M. S. Brandt, M. Stutzmann, S. Koynov, Adv. Energy Mater. 3 (2013) 1068-1074.

[23] C. W. Teplin, B. G. Lee, T. R. Fanning, J. Wang, S. Grover, F. Hasoon, R. Bauer, J. Bornstein, P. Schroeter, H. M. Branz, Energy Environ. Sci. 5 (2012) 8193.

[24] Y. J. Chabal, J. Vac. Sci. Technol., A 7 (1989) 2104.

[25] W. C. Wang, C. W. Lin, H. J. Chen, C. W. Chang, J. J. Huang, M. J. Yang, B. Tjahjono, J. J. Huang, W. C. Hsu, M. J. Chen, ACS Appl. Mater. Interfaces 5 (2013) 9752-9759.

[26] M. Lu, U. Das, S. Bowden, S. Hegedus, R. Birkmire, Prog. Photovoltaics 19 (2011) 326-338.

[27] L. Wang, F. Wang, X. Zhang, N. Wang, Y. Jiang, Q. Hao, Y. Zhao, J. Power Sources 268 (2014) 619-624.

[28] S. Sridharan, N. Bhat, K. N. Bhat, Appl. Phys. Lett. 102 (2013) 021604.

[29] P. Papet, O. Nichiporuk, A. Kaminski, Y. Rozier, J. Kraiem, J. F. Lelievre, A. Chaumartin, A. Fave, M. Lemiti, Sol. Energy Mater. Sol. Cells 90 (2006) 2319-2328.

[30] K. Biswas, S. Kal, Microelectron. J. 37 (2006) 519-525.

[31] E. C. Garnett, P. Yang, J. Am. Chem. Soc. 130 (2008) 9224-9225.

[32] S. De Wolf, M. Kondo, Appl. Phys. Lett.90 (2007) 042111.

Journal of Materials Chemistry A Accepted Manuscript

[33] F. Wang, X. Zhang, L. Wang, Y. Jiang, C. Wei, S. Xu, Y. Zhao, Phys. Chem. Chem. Phys. 16 (2014) 20202-20208.

Journal of Materials Chemistry A Accepted Manuscript

FIGURE CAPTIONS

Fig. 1. SEM images of a Si substrate after (a) NaOH-based pyramidal texturing, (b) annealing at 260°C, and (c) RIE texturing. (d) Cross-sectional view of the local Si MPs+NPs structure. (e) Light absorptions (%) of the planar Si, Si MPs, and Si MPs+NPs hierarchical substrates.

Fig. 2. (a) Schematic of the structure and bandgap of a heterojunction Si solar cell. N-type crystalline Si forms the core of the nanostructure, while the shell consists of an i-a-Si:H passivation layer and a p-a-Si:H emitter layer. (b) EQE characteristics of the Si planar, Si MPs, and Si MPs+NPs hierarchically structured solar cells.

Fig. 3. (a) Minority carrier lifetime curves for the untreated and TMAH-treated Si planar, Si MPs, and Si MPs+NPs substrates. (b) XPS Ag 3d curves of the surfaces of the untreated and treated substrates.

Fig. 4. (a) *J-V* characteristics under illumination of the heterojunction solar cells based on the untreated and treated Si MPs+NPs substrates. (b) EQE of the solar cell based on the treated MPs+NPs substrate. (c) Dark *J-V* characteristics of the heterojunction solar cells based on the treated and untreated Si MPs+NPs substrates.

Journal of Materials Chemistry A Accepted Manuscript

Table 1. Photovoltaic properties of the Si planar, Si MPs, and Si MPs+NPs solar cells

Substrate	V_{oc} *(mV)*	$J_{sc\text{-}qe}$ *(mA/cm²)*	*FF (%)*	*Eff (%)*
Planar Si	576±12	30.4±0.3	69.2±1.3	12.5±0.2
Si MPs	617±11	35.3±0.6	69.7±2.3	15.9±0.3
Si MPs+NPs	557±16	35.8±0.8	67.3±2.8	14.2±0.5

Journal of Materials Chemistry A Accepted Manuscript

Figure 1.

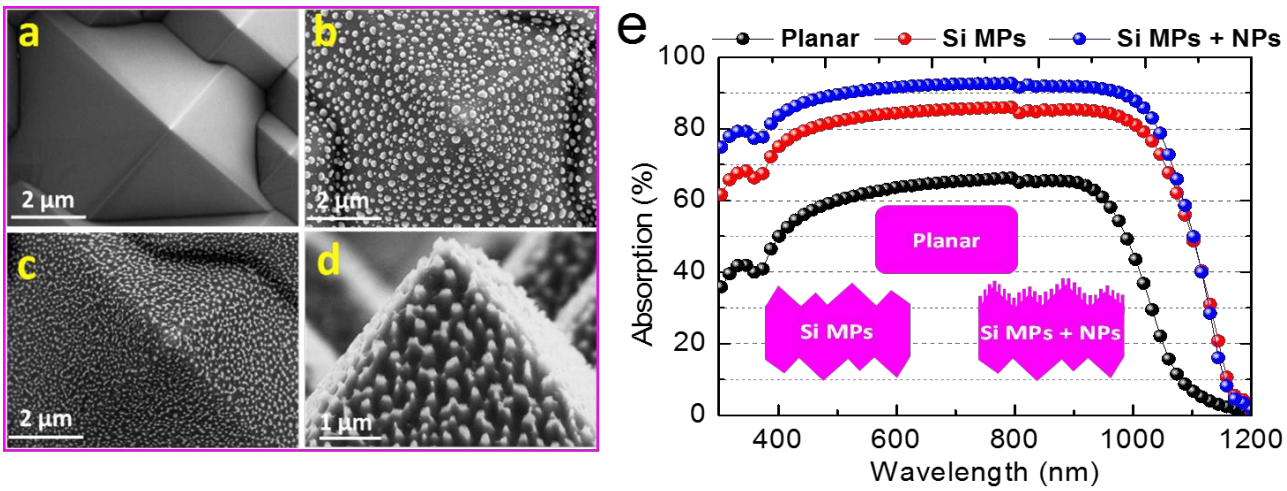

Journal of Materials Chemistry A Accepted Manuscript

Figure 2.

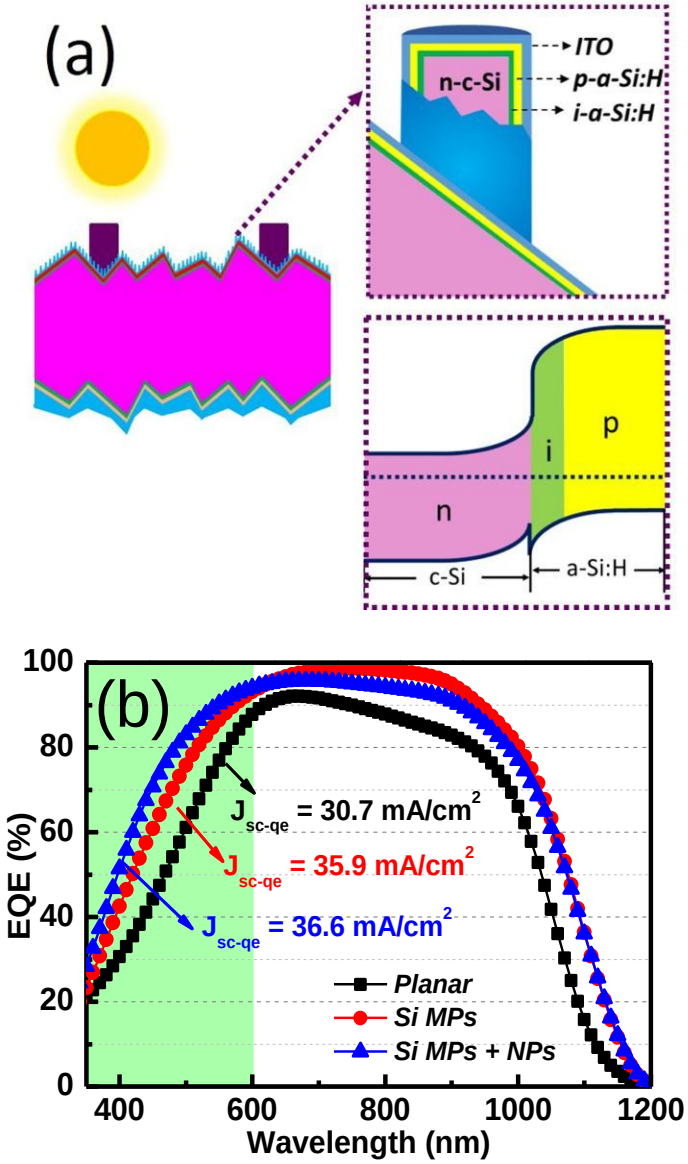

Journal of Materials Chemistry A Accepted Manuscript

Figure 3.

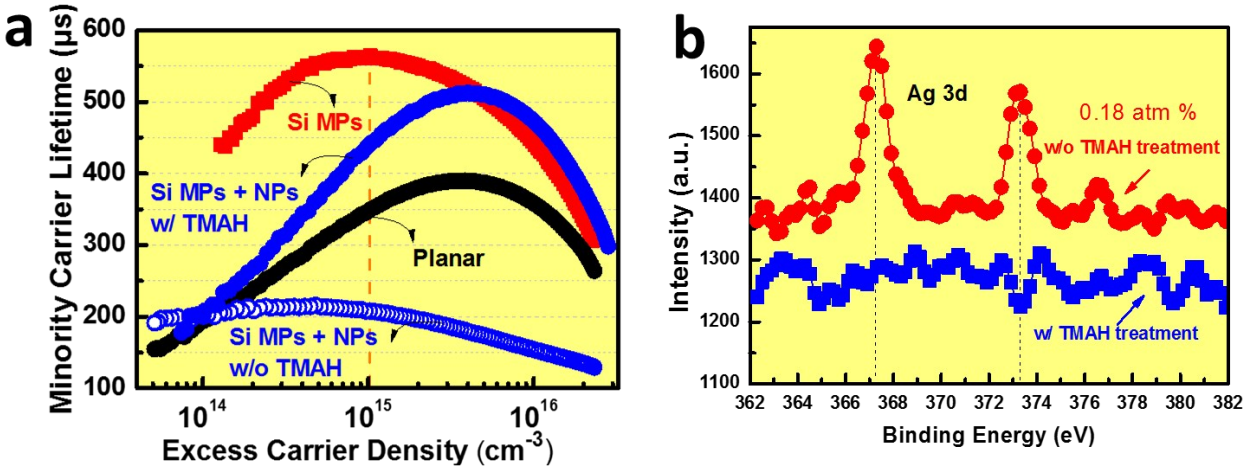

Journal of Materials Chemistry A Accepted Manuscript

Figure 4.

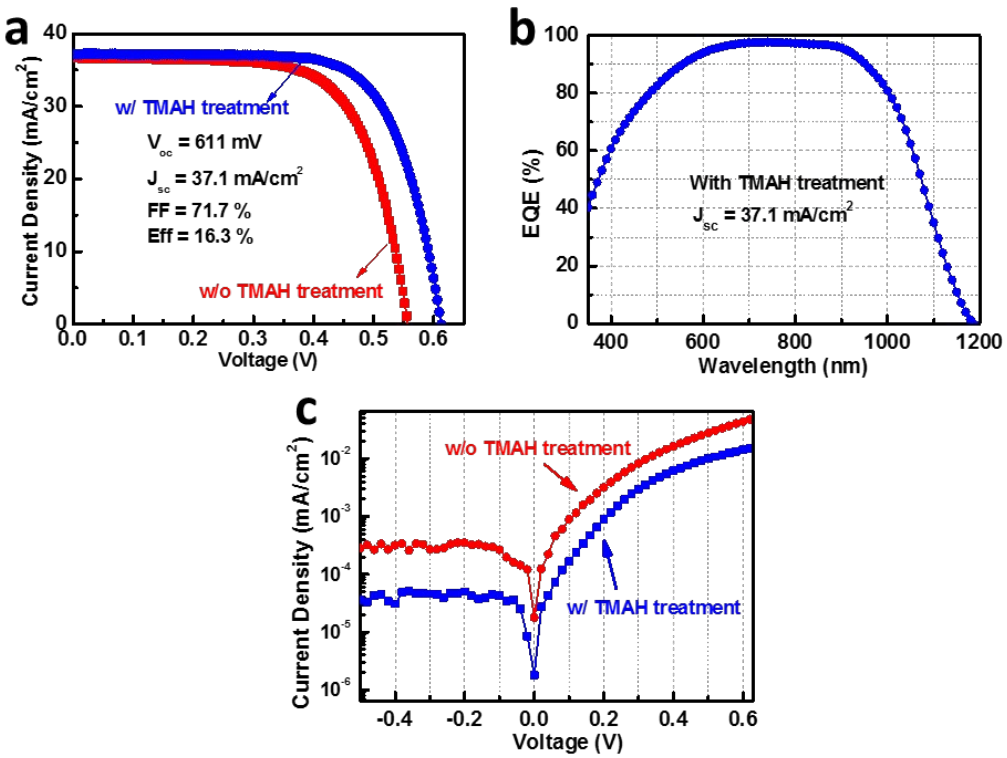

Journal of Materials Chemistry A Accepted Manuscript